International Scholarly Research Network
ISRN Mechanical Engineering
Volume 2011, Article ID 405701, 9 pages
doi:10.5402/2011/405701

Research Article

Boundary Layer Mixture Model for a Microbubble Drag Reduction Technique

Jing-Fa Tsai and Chi-Chuan Chen

Department of Engineering Science and Ocean Engineering, National Taiwan University, No. 1, Section 4, Roosevelt Road, Taipei 10660, Taiwan

Correspondence should be addressed to Jing-Fa Tsai, jftsai@ntu.edu.tw

Received 8 April 2011; Accepted 20 May 2011

Academic Editors: A. E. Huespe and B. Yu

The boundary mixture model is derived to predict the performance of the microbubble drag reduction technique for a flat plate. The flat plate with a porous material microbubble injecting system and resistance-measuring system are set up to measure the frictional resistance of the flat plate without and with injected microbubbles. The tests are conducted in a water tunnel and a towing tank. The test results show that the boundary mixture model predicts the drag reduction well for the flat plate when testing with injected microbubbles in the water tunnel. However, the boundary mixture model overestimates the drag reduction effect for the flat plate tested in the towing tank. The possible mechanism for the overestimation of drag reduction effect in the towing tank may be due to the different behaviors of microbubbles in the velocity gradient of boundary layer.

1. Introduction

The microbubble drag reduction technique has been one of the major research topics both in fluid mechanics and in ship hydrodynamics over the last two decades [1]. Since Madavan et al. [2] achieved an impressive 80% drag reduction in a water tunnel test, many researchers devoted themselves to the study of the microbubble drag reduction technique. The major research directions of the microbubble drag reduction technique include (1) developing the microbubble injection methods and to validate the drag reduction effect in a water tunnel, such as by using the electrolysis method [1], the porous method [2, 3], or the WAIP (winged air induction pipe) method [4], (2) experimentally studying the mechanisms and the key parameters of the microbubble drag reduction technique, such as the bubble size effect [5], the bubble concentration effect [6], the gas type effect [7], or the effect of microbubbles on the structure of turbulence [8], (3) modeling the mechanism of the microbubble drag reduction technique by numerical methods [9] or by DNS simulation [10], and (4) applying the microbubble drag reduction technique to the ship model and conducting the ship model resistance test to study the drag reduction effect in a towing tank [11–13].

Some important research results have emerged for the microbubble drag reduction technique over the last two decades. First, the drag reduction effect of the microbubble in the flat plate was confirmed and an 80% maximum drag reduction effect was also validated in water tunnel tests [2, 3, 14, 15]. Second, it was confirmed that the effect of bubble size (ranging from 0.05 mm to 5 mm) on drag reduction could be neglected [5, 16]. Third, the most important parameter for microbubble drag reduction is the volume fraction of the injected air in the water boundary layer. Skudarnov and Lin [17] also validated the density effect on the drag reduction effect of microbubble drag reduction by using a 2D RANS simulation. But the prediction model for the microbubble drag reduction technique is still not well developed.

In this study, a simple boundary layer mixture model is derived to predict the drag reduction effect of the microbubble drag reduction technique for a flat plate. The flat plate resistance measuring system with a porous material microbubble injecting system is set up to measure the total resistances of the plate without and with injecting

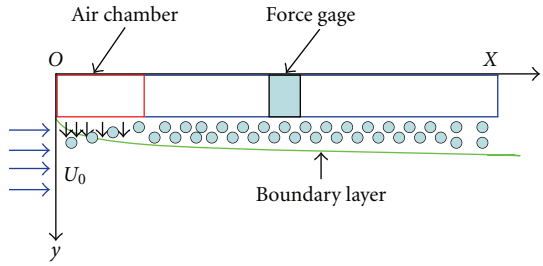

Figure 1: Schematic drawing of a microbubble injecting system (plate on top).

the microbubbles. The tests are conducted in a water tunnel and a towing tank to verify the drag reduction effect predicted by the boundary layer mixture model.

2. Boundary Mixture Model

Figure 1 is a schematic drawing of a microbubble injecting system for a plate on the top. The injected microbubbles are assumed to be distributed uniformly across the boundary layer. The air volume fraction C_v is defined as the ratio of the injected air flow rate divided by the summation of the air flow rate and the water flow rate within the boundary layer,

$$C_v = \frac{Q_a}{Q_a + Q_w}, \tag{1}$$

where Q_a is the injected air flow rate, and Q_w is the water flow rate within the boundary layer of the plate. Based on the turbulent boundary theory [18], the water flow rate within the boundary layer of the plate can be calculated by

$$Q_w = U_0(\delta - \delta^*)b, \tag{2}$$

where b is the width of the plate, U_0 is the inflow velocity, and δ is the boundary layer thickness, which is defined as the distance from the wall where the velocity is $0.99U_0$. A seventh power velocity distribution [18] is assumed for the velocity distribution across the boundary layer

$$\frac{U}{U_0} = \left(\frac{y}{\delta}\right)^{1/7}. \tag{3}$$

And the displacement thickness δ^* is defined as

$$\delta^* = \int_0^\delta \left(1 - \frac{U}{U_0}\right) dy. \tag{4}$$

The Schlichting boundary thickness formula [18] is used to estimate the thickness of the boundary layer

$$\delta = \frac{0.37x}{R_{ex}^{0.2}}, \tag{5}$$

where $R_{ex} = U_0 x/\nu$ and x is the distance from the origin of the plate.

Using (4) and (5) to solve (2), the water flow rate can be calculated by

$$Q_w = 0.3238 U_0 b x R_{ex}^{-0.2}. \tag{6}$$

Then the air volume fraction C_v in (1) can subsequently be calculated with measured injected air flow rate and the water flow rate which was estimated by using (6).

For a flat plate without injected bubbles, the frictional resistance D_f of a flat plate with length l and width b can be derived as [18]

$$D_f = 0.036 \rho_w U_0^2 l^2 b R_{el}^{-0.2}, \tag{7}$$

where $R_{el} = U_0 l/\nu$ and l is the total length of the plate, and ρ_w is the density of the water.

The resistance coefficient C_f is defined as

$$C_f = \frac{D_f}{0.5 \rho_w U_0^2 l b} = 0.074 l R_{el}^{-0.2}. \tag{8}$$

For the water-bubble mixture of the boundary layer with injected bubbles, the mixture density ρ_b can be calculated by the linear combination of the density of air and the density of water according to the air volume fraction C_v, and is given by

$$\rho_b = \frac{\rho_a Q_a + \rho_w Q_w}{Q_a + Q_w} = \rho_a C_v + \rho_w (1 - C_v), \tag{9}$$

where ρ_a is the density of the injected air.

The dynamic viscosity of the water-bubble mixture can also be calculated by using the same approach as

$$\mu_b = \frac{\mu_a Q_a + \mu_w Q_w}{Q_a + Q_w} = \mu_a C_v + \mu_w (1 - C_v). \tag{10}$$

The kinematical viscosity of the water-bubble mixture ν_b is then defined as

$$\nu_b = \frac{\mu_b}{\rho_b}. \tag{11}$$

The frictional resistance of a flat plate with a water-bubble mixture boundary layer D_{fb} can be calculated by using the same approach [18] as

$$D_{\text{fb}} = 0.036 \rho_b U_0^2 l^2 b R_{ebl}^{-0.2}, \tag{12}$$

where the Reynolds number of the water-bubble mixture R_{ebl} is defined as

$$R_{ebl} = \frac{U_0 l}{\nu_b}. \tag{13}$$

The ratio of the frictional resistance of water-bubble mixture to the frictional resistance of the water is then expressed as

$$\frac{D_{\text{fb}}}{D_f} = \frac{\rho_b R_{ebl}^{-0.2}}{\rho_w R_{el}^{-0.2}}. \tag{14}$$

Equation (14) predicts the frictional resistance of water-bubble mixture of the plate from the frictional resistance of flat plate in pure water.

If the frictional resistances D_{fb} and D_f are normalized by the dynamic pressure of the inflow $(1/2)\rho_w U_0^2$ and the surface

Table 1: Density and Reynolds number effect on the microbubble drag reduction.

C_v	ρ_b/ρ_w	$R_{ebl}^{-0.2}/R_{el}^{-0.2}$	C_{fb}/C_f	DR
0.000	1.000	1.000	1.000	0.000
0.100	0.900	1.000	0.900	0.100
0.200	0.800	1.001	0.801	0.199
0.300	0.700	1.001	0.701	0.299
0.400	0.600	1.002	0.602	0.398
0.500	0.501	1.003	0.502	0.498
0.600	0.401	1.004	0.402	0.598
0.700	0.301	1.006	0.303	0.797
0.800	0.201	1.011	0.203	0.897
0.900	0.101	1.024	0.103	0.997
0.990	0.011	1.174	0.013	0.987

area of the flat plate $b * l$, then the same result will be had for the nondimensional resistance coefficients as will be

$$\frac{C_{\text{fb}}}{C_f} = \frac{\rho_b R_{ebl}^{-0.2}}{\rho_w R_{el}^{-0.2}}, \tag{15}$$

where $C_f = D_f/(1/2)\rho_w U_0^2 lb$ and $C_{\text{fb}} = D_{\text{fb}}/(1/2)\rho_w U_0^2 lb$.

Equation (15) predicts the nondimensional frictional resistance of water-bubble mixture of the plate from the nondimensional frictional resistance of flat plate in water. The drag reduction ratio DR predicted by the boundary layer mixture model can be calculated by

$$\text{DR} = 1 - \frac{C_{\text{fb}}}{C_f}. \tag{16}$$

Figure 2 shows the ratio of nondimensional resistance coefficients of the bubble-water mixture to the pure water with the parameter of the air volume fraction and the drag reduction ratio. The effect of the density of the mixture and Reynolds number on the microbubble drag reduction technique is shown in Table 1. The effect of the Reynolds number is very small when compared with the effect of density of the mixture. The density of the bubble mixture becomes the key parameter for the microbubble drag reduction technique. The ratio of the frictional resistance of the water-bubble mixture boundary layer to the water boundary layer is almost directly proportional to the density ratio.

3. Experimental Apparatus and Test Procedures

Figure 3 shows a flat plate resistance measuring system. The length of the flat plate is 700 mm and the width is 190 mm. The flat plate is suspended by four steel strips at the four corners. The force gage is located at the center of the plate to measure the resistance of the suspended flat plate. Figure 4 shows a porous plate microbubble injecting system, which is designed to inject the microbubbles through the porous plate. The length of the porous plate is 120 mm and the width is 190 mm. The pore sizes of porous plate used in the water tunnel test are 10 μm and 100 μm. The microbubble injecting system is placed in front of the flat plate resistance measuring system, and they are combined together as a whole unit. Figure 5 shows the whole system installed in the water tunnel. The water tunnel is the K23 cavitation tunnel from K&R Germany.

The resistances of the flat plate without injecting microbubbles are first measured for different velocities varying from 2.45 m/s to 4.2 m/s. The resistances of the flat plate while injecting microbubbles are then measured for different air flow rates for each velocity. The air flow rates range from 12 L/min to 75 L/min.

The same system is also installed at the towing carriage to conduct the resistance test in the towing tank. The dimensions of the towing tank are 130 m in length, 8 m in width, and 4 m in depth. The maximum speed of the towing carriage is 5 m/s. Figure 6 shows the flat plate resistance measuring system with the towing carriage in the towing tank. The test procedure and conditions in the towing tank are the same as in the water tunnel.

4. Test Results and Validation of the Boundary Layer Mixture Model

Figure 7 shows the measured resistance coefficients of the flat plate without injecting microbubbles tested in the water tunnel and in the towing tank. The measured resistance coefficients are about the same, both in the water tunnel and in the towing tank. The resistance coefficient calculated by the formula (8) is also shown in Figure 7. The measured resistance coefficients of the flat plate both from the water tunnel and the towing tank are a little higher than the resistance coefficients predicted by the formula (8). It is reasonably common to achieve a higher resistance in the test environment than when using the formula because of the imperfection of the flat plate test setup and the three-dimensional effects.

Figure 8 shows the resistance coefficient ratio of the flat plate with the injected microbubbles by a 10 μm porous plate and without the injected microbubbles tested in the water tunnel. The measured resistance coefficient ratio is in good agreement with the drag reduction line predicted by the boundary mixture model. Figure 9 shows the resistance coefficient ratio of the flat plate with the injected microbubbles by a 100 μm porous plate and without the injected microbubbles tested in the water tunnel. The measured resistance coefficient ratio of the 100 μm porous plate is also in good agreement with the frictional resistance line predicted by the boundary mixture model.

Figure 10 shows the resistance coefficient ratio of the flat plate with the injected microbubbles by a 10 μm porous plate and without the injected microbubbles tested in the towing tank. The drag reduction effect of the 10 μm porous plate in towing tank is much smaller then that predicted by the boundary mixture model. Figure 11 shows the resistance coefficient ratio of the flat plate with the injected microbubbles by a 100 μm porous plate and without the injected microbubbles tested in the towing tank. The drag reduction effect of the 100 μm porous plate in towing tank

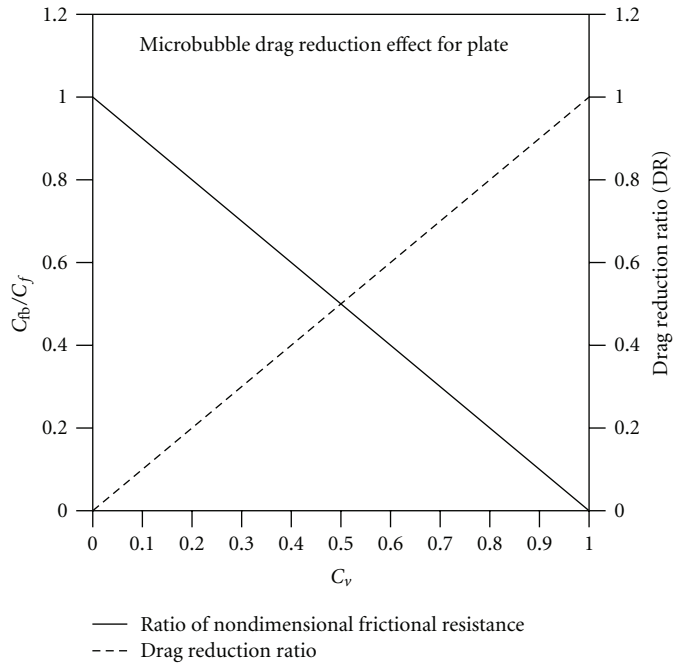

Figure 2: The drag reduction effect predicted by the boundary layer mixture model.

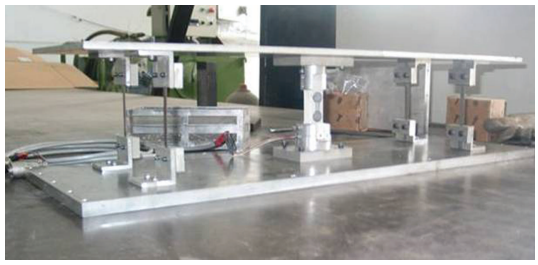

Figure 3: The flat plate resistance measuring system.

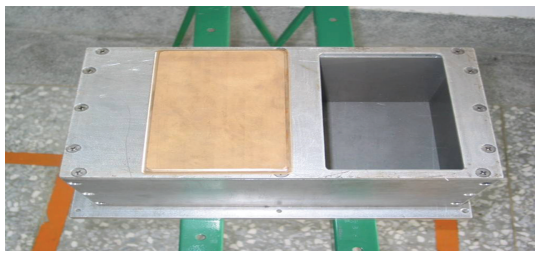

Figure 4: Air chamber and porous plate (the yellow one).

Figure 5: The whole microbubble resistance measuring system in water tunnel.

Figure 6: The whole microbubble resistance measuring system in towing tank.

is also much smaller then that predicted by the boundary mixture model. In addition, the drag reduction effect is decreased at a higher air flow rate for velocities 2.45 m/s and 2.9 m/s. For example, at a velocity 2.45 m/s, the resistance ratio is 0.77 when the air volume fraction is 0.65, but the resistance ratio is 0.85 when the air volume fraction is 0.71. The drag reduction effect is decreased from 23% to 15% when the air volume fraction is increased from 0.65 to 0.71. This implies that there exits an optimal air flow rate

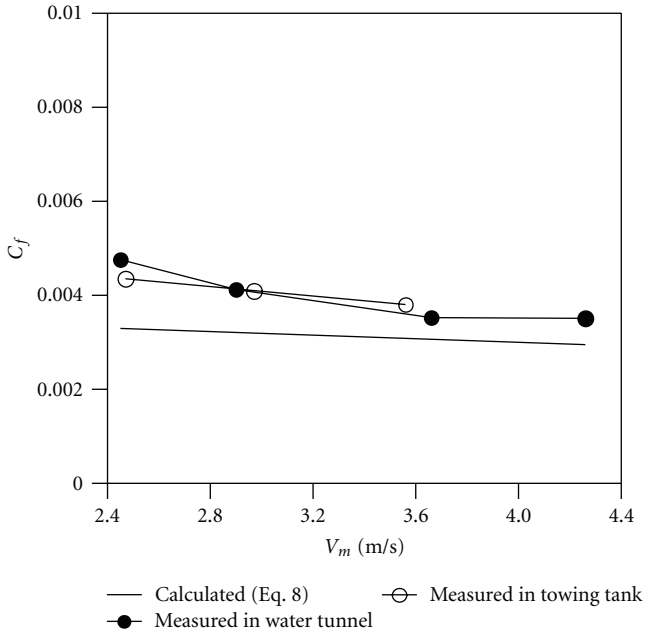

Figure 7: Resistance of flat plate without injected microbubbles.

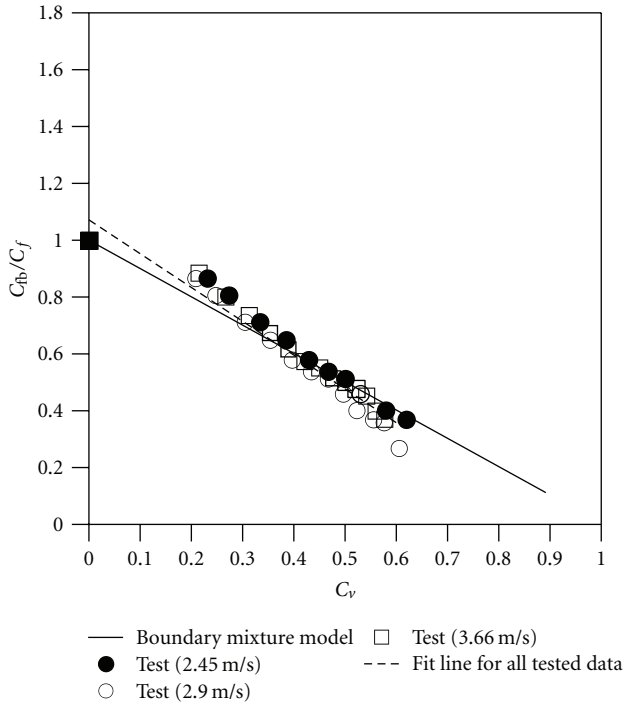

Figure 8: The drag reduction ratio of the flat plate with a 10 μm porous plate injecting microbubbles in the water tunnel.

when using the microbubble drag reduction technique in the towing tank for each velocity. This trend is different from the air flow rate increasing monotonically with increasing the drag reduction effect in the water tunnel.

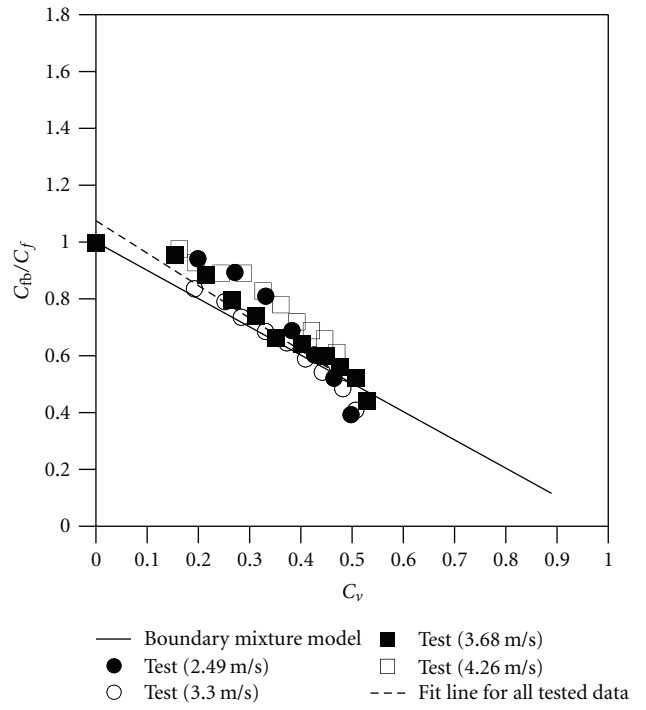

Figure 9: Drag reduction ratio of the flat plate with a 100 μm porous plate injecting microbubbles in the water tunnel.

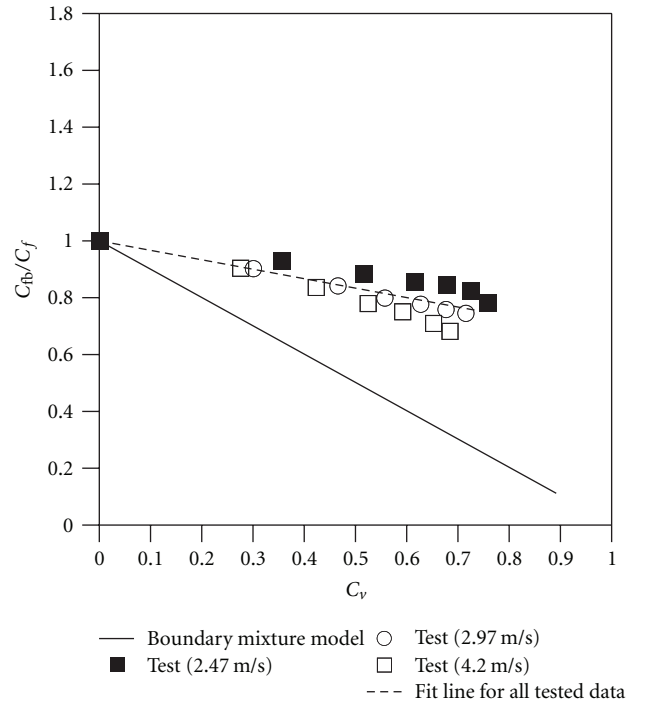

Figure 10: Drag reduction ratio of the flat plate with a 10 μm porous plate injecting microbubbles in the towing tank.

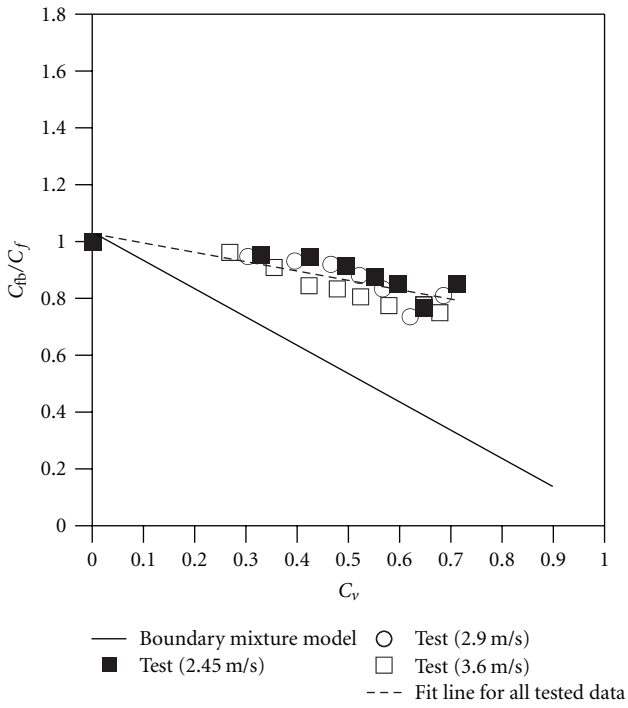

Figure 11: Drag reduction ratio of the flat plate with a 100 μm porous plate injecting microbubbles in the towing tank.

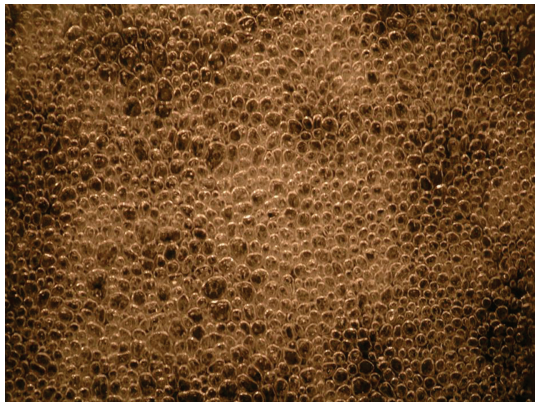

Figure 12: Microbubble distribution across the flat plate in the water tunnel.

5. Discussions

The test results show some differences for the microbubble drag reduction technique tested in the water tunnel and in the towing tank. The first is that the maximum drag reduction effect of the microbubbles in the water tunnel is about 80%, and the drag reduction effect is in good agreement with the value predicted by the boundary mixture model. However, in this study, the maximum drag reduction effect of microbubble in the towing tank is only about 30%. Takahashi et al. [19] only achieved a 22% drag reduction for a 50-meter flat plate ship in the towing tank. The second is that the drag reduction effect increases monotonically with an increasing the air flow rate in the water tunnel.

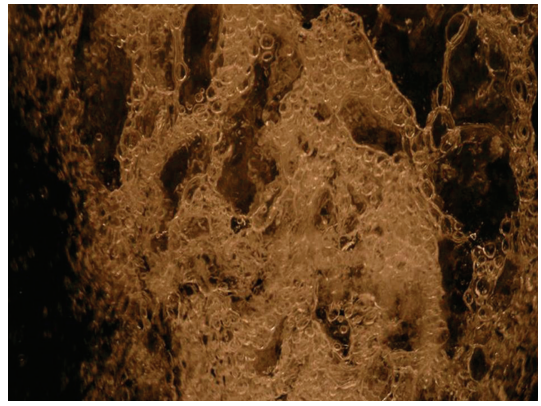

Figure 13: Microbubble distribution across the flat plate in the towing tank.

However, an optimal air flow rate exists in the towing tank. The drag reduction effect will be decreased when the air flow rate is above a critical air flow rate. The third is that the drag reduction effect is only a function of the air volume fraction C_v and is independent of velocity in the water tunnel. Madavan et al. [2] showed the same trend in which the drag reduction is only a function of nondimensional air flow rate $C_q = Q_a/(U_0 A)$ in water tunnel. However, in the towing tank, the drag reduction effect is slightly dependent on velocity as shown in Figures 10 and 11.

The mechanism that creates the difference in the drag reduction effect of the flat plate when it is tested between the water tunnel and the towing tank plays a crucial role for the application of microbubble drag reduction technique in ships. The most likely mechanism may be the different behaviors of microbubbles between in the water tunnel and in the towing tank. A transparent acrylic plate is used instead of the steel plate of the resistance measuring system to observe the microbubble behaviors in the water tunnel and in the towing tank. Figure 12 shows the distribution of microbubbles in the water tunnel. The microbubbles are distributed uniformly across the whole plate, and the individual bubbles can be seen clearly. Figure 13 shows the bubble distribution across the flat plate in the towing tank. The bubbles are deformed irregularly, and many bubbles are attached to the plate. The irregular black holes in Figure 13 are large deformed bubbles attached to the plate. There are more like an air packets for the white bubbles as shown in Figure 13.

The different behaviors of bubbles in the water tunnel and in the towing tank may be due to the different velocity gradient in the boundary layer. The bubble will suffer a lift force when it remains in the velocity gradient. Figure 14 shows a schematic diagram for a bubble of radius R being lifted by a velocity gradient. The lift force can be calculated by

$$F_L = \rho_w V C_L \vec{U} \times \varpi_0 \,, \tag{17}$$

where V is the volume of the bubble, $\varpi_0 = \nabla \times \vec{U}$ is calculated at the bubble center, and C_L is the lift coefficient.

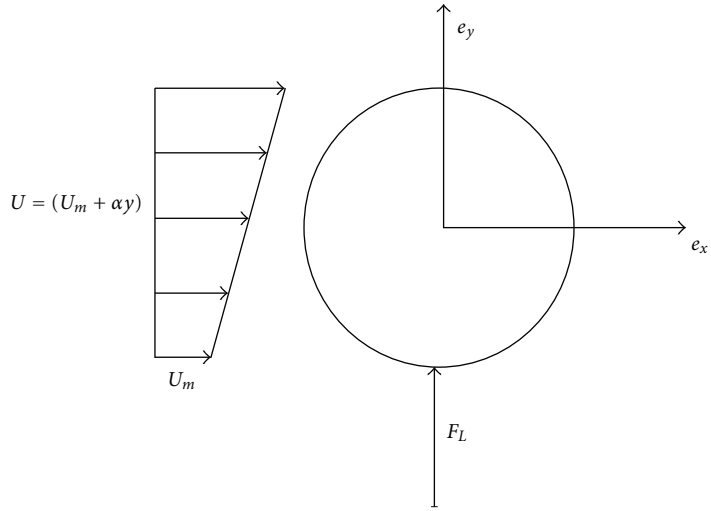

Figure 14: Bubble's lift force produced by a velocity gradient.

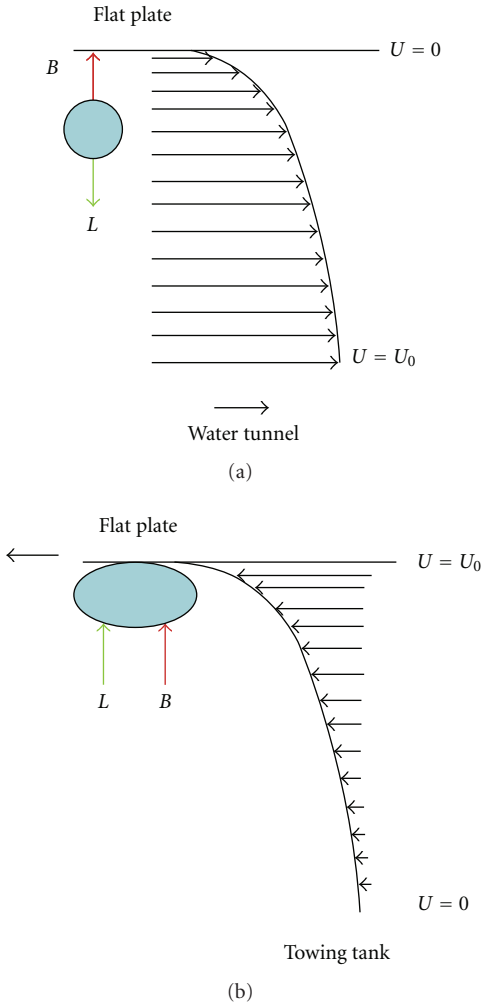

Figure 15: Forces of a bubble suffered in the boundary layer of the water tunnel and the towing tank.

For an inviscid fluid satisfying the nondimensional shear rate $S_r = 2R\alpha/U_m \ll 1$, Auton et al. [20] obtained the lift force as

$$F_L = \frac{2}{3}\pi\rho_w R^3 \alpha U_m \,, \tag{18}$$

where α is the linear slope of the velocity gradient across the bubble and U_m is the minimum velocity of the bubble encountered.

The direction of the lift force is from the low velocity to the high velocity.

Besides the lift force, the bubble also has a buoyancy force in the upward direction. Figure 15 shows the velocity gradients of the boundary layer both in the water tunnel and in the towing tank. For the water tunnel, the flat plate is fixed at the top of the water tunnel wall, the velocity of the flat plate is zero, and the velocity outside the boundary of the flat plate is U_0. Because the microbubble is injected into the boundary layer, it will suffer a velocity gradient and produce a lift force with a downward direction and an upward buoyancy force. The two forces could be balanced in some situations, so the bubble could stay in the buffer layer [21] and will not attach to the surface of the flat plate as shown in Figure 15(a).

For the flat plate installed in the towing tank, the flat plate moves with the speed U_0 of the towing carriage. The speed of the water outside the boundary layer of the plate is zero. The velocity gradient of the boundary layer in the towing tank is reversed when compared with the velocity gradient in the water tunnel. The direction of the bubble's lift force produced by the velocity gradient as well as the direction of the bubble's buoyancy is upward in the towing tank. The two forces will push the bubble toward the surface of the flat plate, and the bubbles will attach to the surface of the flat plate as shown in Figure 15(b). The bubbles will be accumulated at the surface of the plate. In addition, the coalescence of bubbles occurs at the surface of the plate and forms several large flat bubbles attached to the surface of the moving flat plate, which can be seen in Figure 13. The resistance of the flat plate is increased

when a large deformed bubble is attached to its surface. Also, the drag reduction effect is decreased. Future study is required to examine the detailed process of the injected bubble to forming an irregular large bubble and attaching to the flat plate surface in the towing tank.

6. Conclusions

A boundary layer mixture model was derived to predict the drag reduction effect of microbubble drag reduction technique in the flat plate. Also, a flat plate total drag measurement with microbubble injecting system was designed to conduct the resistance test in the water tunnel as well as in the towing tank. From the prediction of the boundary mixture model, the test results, and the discussions, the following conclusions can be drawn.

(1) The drag reduction effect predicted by the boundary mixture model is almost directly proportional to the density ratio of mixture and water.

(2) The maximum drag reduction effect of the microbubbles in water tunnel is about 80%, and the frictional resistance coefficient is in good agreement with the value predicted by the boundary mixture model. The maximum drag reduction effect of the microbubbles in the towing tank is only about 30% and drag reduction is much smaller than that predicted by the boundary mixture model.

(3) The drag reduction effect increases monotonically with increasing the air flow rate in the water tunnel. However, an optimal air flow rate exists for each velocity in the towing tank.

(4) The different drag reduction effect in the water tunnel and in the towing tank may be due to the different bubble behaviors produced by the different velocity gradient. Future study is required to examine the details of the developing process of the injected bubble in the towing tank.

Nomenclatures

A: Area of the porous plate
b: Breadth of the flat plate
C_f: Frictional resistance coefficient of the flat plate in water
C_{fb}: Frictional resistance coefficient of the flat plate in bubble-water mixture
C_L: Lift coefficient of bubble in velocity gradient
C_q: Nondimensional air flow rate
C_v: Air volume fraction
D_f: Frictional resistance of the flat plate in water
D_{fb}: Frictional resistance of the flat plate in bubble-water mixture
DR: Drag reduction ratio
F_L: Lift of a bubble in velocity gradient
l: Length of the flat plate
R: Radius of a bubble
R_{el}: Reynolds number of flat plate with length l in water
R_{ebl}: Reynolds number of flat plate with length l in bubble-water mixture
R_{ex}: Reynolds number at any x coordinate of flat plate in water
S_r: Nondimensional shear rate of a bubble
U: Velocity component in x axes within the boundary layer of the flat plate
U_0: Uniform inflow velocity outside boundary layer of the flat plate
U_m: Minimum velocity of a bubble experienced within the diameter of the bubble
V: Volume of a bubble
x: Coordinate of horizon axes along the flat plate
y: Coordinate of vertical axes perpendicular to the flat plate
α: Slope of velocity within the range of bubble's diameter
ρ_a: Density of air
ρ_b: Density of bubble-water mixture
ρ_w: Density of water
μ_a: Dynamic viscosity of air
μ_b: Dynamic viscosity of bubble-water mixture
μ_w: Dynamic viscosity of water
ν_a: Kinematical viscosity of air
ν_b: Kinematical viscosity of bubble-water mixture
ν_w: Kinematical viscosity of water
δ: Boundary layer thickness
δ^*: Boundary layer displacement thickness
ω_0: Vorticity of a bubble within a velocity gradient.

Acknowledgment

The authors are grateful for the funding support of the National Science Council of Taiwan (NSC92-2611-E-002-022).

References

[1] M. E. McCormick and R. Bhattacharyya, "Drag reduction of a submersible hull by electrolysis," *Naval Engineers Journal*, vol. 85, no. 2, pp. 11–16, 1973.

[2] N. K. Madavan, S. Deutsch, and C. L. Merkle, "Reduction of turbulent friction by microbubbles," Technical Memorandum TM 83-23, The Pennsylvania State University, 1983.

[3] W. C. Sanders, S. L. Ceccio, E. M. Ivy, M. Perlin, and D. R. Dowling, "Microbubble drag reduction at high Reynolds number," in *Proceedings of the 4th ASME/JSME Joint Fluids Engineering Conference*, pp. 683–695, Honolulu, Hawaii, USA, July 2003.

[4] I. Kumagai, N. Nakamura, Y. Murai, Y. Tasaka, Y. Takeda, and Y. Takahashi, "A new power-saving device for air bubble generation: hydrofoil air pump for ship drag reduction," in *Proceedings of the International Conference on Ship Drag Reduction SMOOTH-SHIPS*, Istanbul, Turkey, May 2010.

[5] X. Shen, S. L. Ceccio, and M. Perlin, "Influence of bubble size on micro-bubble drag reduction," *Experiments in Fluids*, vol. 41, no. 3, pp. 415–424, 2006.

[6] M. M. Guin, H. Kato, H. Yamaguchi, M. Maeda, and M. Miyanaga, "Reduction of skin friction by microbubbles and its relation with near-wall bubble concentration in a channel," *Journal of Marine Science and Technology*, vol. 1, no. 5, pp. 241–254, 1996.

[7] A. A. Fontaine and S. Deutsch, "The influence of the type of gas on the reduction of skin friction drag by microbubble injection," *Experiments in Fluids*, vol. 13, no. 2-3, pp. 128–136, 1992.

[8] H. Kato, T. Iwashina, M. Miyanaga, and H. Yamaguchi, "Effect of microbubbles on the structure of turbulence in a turbulent boundary layer," *Journal of Marine Science and Technology*, vol. 4, no. 4, pp. 155–162, 2000.

[9] N. K. Madavan, C. L. Merkle, and S. Deutsch, "Numerical investigation into the mechanisms of microbubble drag reduction," *Journal of Fluids Engineering*, vol. 107, no. 3, pp. 370–377, 1985.

[10] K. Sugiyama, T. Kawamura, S. Takagi, and Y. Matsumoto, "Numerical simulations on drag reduction mechanism by microbubbles," in *Proceeding of the 3rd Symposium on Smart Control of Turbulence*, pp. 129–139, University of Tokyo, Japan, 2002.

[11] R. Latorre, "Ship hull drag reduction using bottom air injection," *Ocean Engineering*, vol. 24, no. 2, pp. 161–175, 1997.

[12] Y. Kodama, T. Takahashi, M. Makino, T. Hori, and T. Ueda, "Practical application of microbubbles to ships—large scale model experiments and a new full scale experiment," in *Proceedings of the 6th International Symposium on Smart Control of Turbulence*, Tokyo, Japan, March 2005.

[13] C. Thill, S. Toxopeus, and F. van Walree, "Project Energy-saving air-Lubricated Ships (PELS)," in *Proceedings of the 2nd International Symposium on Seawater Drag Reduction*, Busan, Korea, May 2005.

[14] H. Kato, M. Miyanaga, and H. Yamaguchi, "Frictional drag reduction by injecting bubbly water into a turbulent boundary layer and the effect of plate orientation," in *Cavitation and Gas-Liquid Flow in Fluid Machinery and Device, FED*, vol. 190, pp. 185–194, ASME, 1994.

[15] J. F. Tsai and C. C. Chen, "Experimental study on the micro-bubble drag reduction effect in water tunnel and towing tank," in *Proceedings of the 3rd Asia-Pacific Workshop on Marine Hydrodynamics (APHydro '06)*, Shanghai, China, June 2006.

[16] T. Kawamura, A. Kakugawa, Y. Kodama, Y. Moriguchi, and H. Kato, "Controlling the size of microbubbles for drag reduction," in *Proceeding on 3rd Symposium on Smart Control of Turbulence*, pp. 129–139, University of Tokyo, Japan, 2002.

[17] P. V. Skudarnov and C. X. Lin, "Drag reduction by gas injection into turbulent boundary layer: density ratio effect," *International Journal of Heat and Fluid Flow*, vol. 27, no. 3, pp. 436–444, 2006.

[18] H. Schlichting, *Boundary-Layer Theory*, McGraw-Hill, 6th edition, 1968.

[19] T. Takahashi, A. Kakugawa, M. Makino, and Y. Kodama, "Experimental study on scale effect of drag reduction by microbubbles using very large flat plate ships," *Journal of the Kansai Society of Naval Architects*, no. 239, pp. 11–20, 2003.

[20] T. R. Auton, J. C. R. Hunt, and M. Prud'homme, "Force exerted on a body in inviscid unsteady non-uniform rotational flow," *Journal of Fluid Mechanics*, vol. 197, pp. 241–257, 1988.

[21] J. Ortiz-Villafuerte and Y. A. Hassan, "Investigation of microbubble boundary layer using particle tracking velocimetry," *Journal of Fluids Engineering*, vol. 128, no. 3, pp. 507–519, 2006.